Development of Solid-State Disk Laser for High-Average Power

John Vetrovec,[a] Andrea Koumvakalis, Rashmi Shah, and Tom Endo

Lasers & Electro-Optics Systems, The Boeing Company
6633 Canoga Avenue, Canoga Park, CA. 91309, USA

ABSTRACT

This work describes recent progress in the development of solid-state laser using a composite disk in the active mirror configuration. Pump diode arrays are placed around the perimeter of the disk and pump light is injected into the undoped edge. Uniform laser gain can be achieved with proper choice of lasant doping level, diode placement, and diode divergence. Effective reduction of thermo-optical distortions makes this laser suitable for pulse amplification at high-average power.

Keywords: Solid-state laser, disk laser, active mirror, edge pumping

1. INTRODUCTION

Disk-type solid-state laser (SSL) is recognized for its inherently low susceptibility to thermo-optical distortions (see e.g., [1]). Its large, round aperture reduces diffraction and beam clipping losses experienced by other SSL configurations. These attributes make the disk laser an attractive candidate for large size, high-efficiency systems producing high quality beams. Disk lasers are being developed world-wide primarily as giant pulse amplifiers for nuclear fusion research. A "reflective" version of the laser disk, also known as active mirror amplifier (AMA) has a large surface available for liquid cooling, which makes it particularly suitable for operation at high-average power (HAP). A version of AMA known as "thin disk laser" is now being investigated in Germany [2] and at the Lawrence Livermore National Laboratory in the United States [3]. Recently, we reported the development of a new disk laser concept known as the compact active mirror laser (CAMIL) [4,5]. In this work, we will describe further development of CAMIL with pump radiation injected into the edge of the disk.

2. COMPACT ACTIVE MIRROR LASER (CAMIL)

CAMIL uses a large-aperture laser gain medium disk mounted on a rigid, cooled substrate, Figures 1 and 2. The laser disk is about 2.5 mm in-thickness with a diameter typically between 5 and 15 cm. The disks material can be yttrium aluminum garnet (YAG), gadolinium gallium garner (GGG), glass, or other host media doped with Nd or Yb ions. The substrate contains a built-in heat exchanger with microchannels on the front surface so that coolant can directly wet the back face of the laser medium disk. Except for the microchannel penetrations, the front surface of the substrate is machined to optical flatness. The disk is attached to the substrate by a hydrostatic pressure differential between the surrounding atmosphere and the coolant fluid in the microchannels. This method of attachment maintains the disk in an optically flat condition. CAMIL modules can be used to construct laser amplifiers and oscillators for operation at HAP.

Edge-pumped CAMIL uses a composite disk produced by diffusion bonding of undoped crystal to the peripheral edges of a doped crystal [5]. This construction improves coupling between the pump diodes and the gain medium, aids concentration of pump radiation, provides cooling to the doped disk edge, and helps to suppress parasitic oscillations by providing a trap for amplified spontaneous emission (ASE). Diode pump arrays are arranged around the circumference of the composite disk and generally point toward its center. Pump radiation is first focused by the curved input surface and concentrated in the tapered portion of the undoped crystal, followed by injection into the perimeter edge of the doped disk, Figure 3. Aided by multiple internal reflections, pump radiation

[a] jan.vetrovec@boeing.com tel. (818) 586-3101, fax (818) 586-3074

is channeled into and through the doped portion of the disk where it is gradually absorbed. Edge-pumping is very advantageous because it provides a long absorption path for the pump, which allows reduction of disk doping level and makes it more practical to use lasants with low absorption cross-sections. Peripheral edge of the doped disk receiving highest pump intensity is susceptible to overheating and, as a result, to excessive thermal stresses. The undoped edge draws heat away from the peripheral edge of the doped disk and conducts it to the heat exchanger. This avoids high thermal stresses and phase front distortions near the edge of the doped disk, and permits power extraction from nearly 100% of the disk volume.

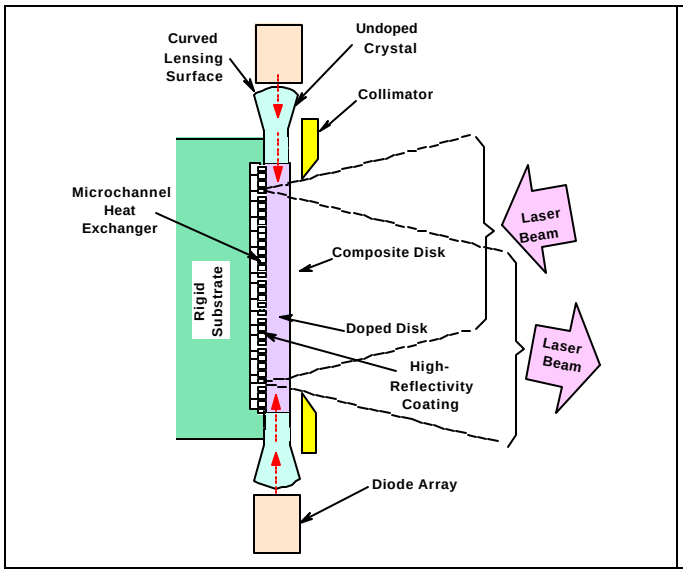

Figure 1: Edge-pumped CAMIL disk

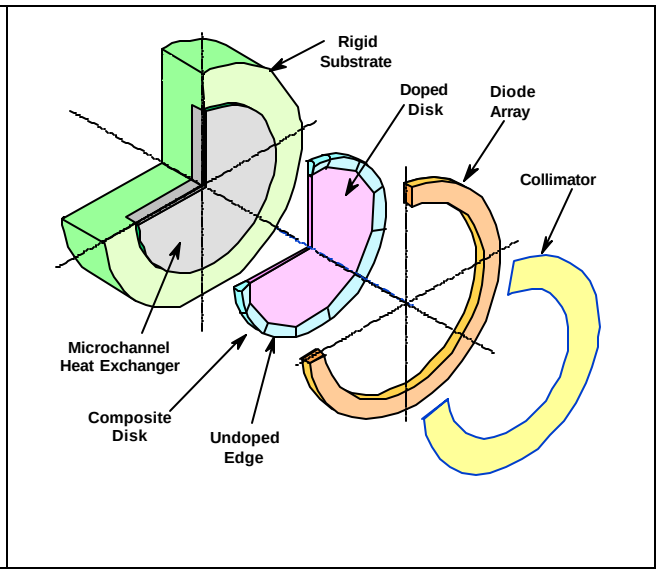

Figure 2: Exploded view of edge-pumped CAMIL

One key advantage of CAMIL is its scalability over a broad range of average laser powers [6]. In particular, power scaling can be accomplished by increasing the disk size and/or by increasing the number of disks in the laser. For any given disk size, the maximum average laser power is also limited by thermal fracture of the disk and by ASE losses. Figure 4 shows the power scaling of CAMIL disk using Nd and Yb lasants doped into YAG and GGG operated under these limiting conditions.

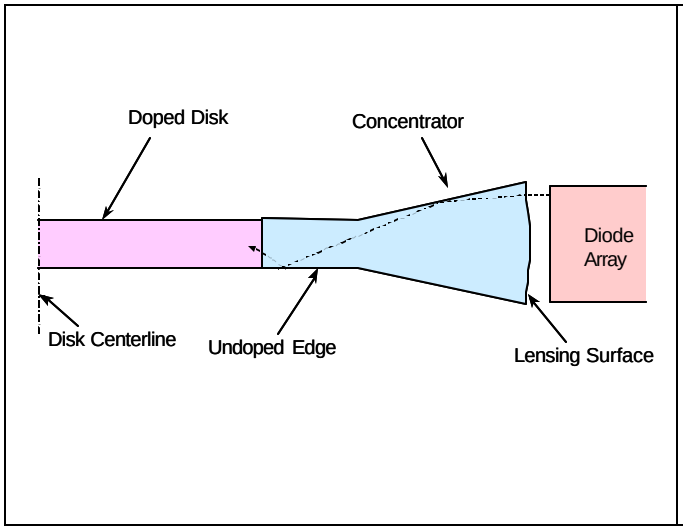

Figure 3: Rays emitted by diode array are traped by TIR and transported into the doped disk

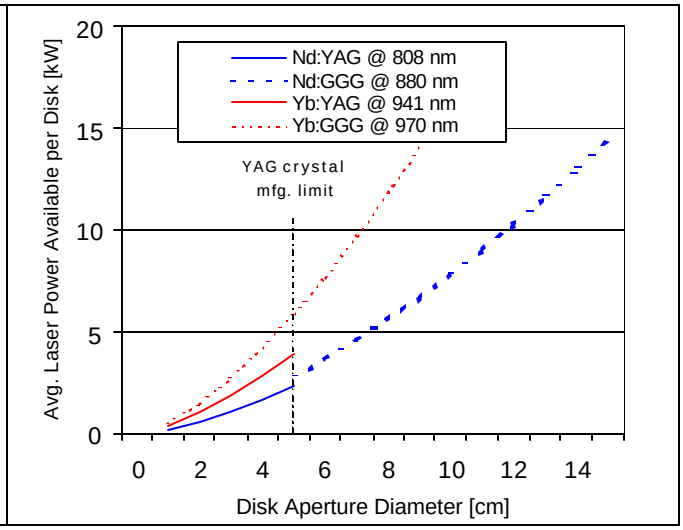

Figure 4: Power scaling of CAMIL with Nd and Yb in YAG and GGG under several pump conditions

3. PUMP DIODE MODEL

A laser diode emits optical radiation from a surface approximately 1-2 μm high and about 100-200 μm wide. A beamlet of radiation emitted from this surface is very asymmetric: highly divergent in a direction parallel to the 1-2 μm dimension (so called "fast axis") and moderately divergent in the transverse dimension (so-called "slow axis"), Figure 5. Typical fast axis divergence angles (full-width at half-maximum intensity, FWHM) range from 30 to 60 degrees, while slow axis divergence angles typically range from 8 to 12 degrees. Spatial profile of individual beamlets is approximately bi-Gaussian. To investigate the spatial distribution of diode light, the output of an individual diode can be approximated by a Gaussian point emitter. The far-field intensity profile of a beamlet generated by a bi-Gaussian point emitter of strength (power) P_0 can be described in the coordinate system (u,v,w) of the emitter as

$$p(u,v,w) = \frac{P_o}{\pi w^2 \theta_o \varphi_o} \exp -\left(\frac{u}{\varphi_o w}\right)^2 \exp -\left(\frac{v}{\theta_o w}\right)^2 \qquad (1)$$

where φ_o and θ_o are divergence angles of a bi-Gaussian beam (half width at maximum/e), Figure 6. Note that the relationship between FWHM divergence and "Gaussian" divergence is $\varphi_{FWHM} = 2\,\varphi_G\,(\ln 2)^{1/2} \approx 1.67\,\varphi_G$.

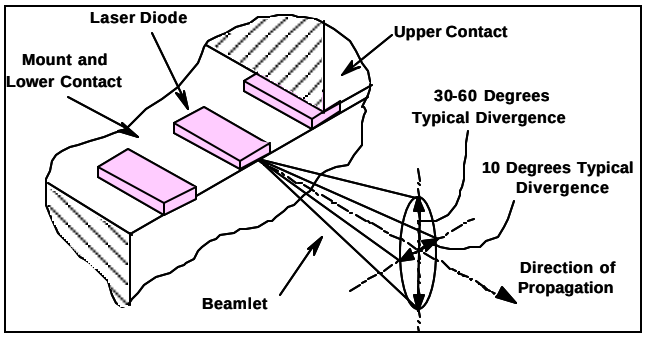

Figure 5: Beamlet produced by individual diodes

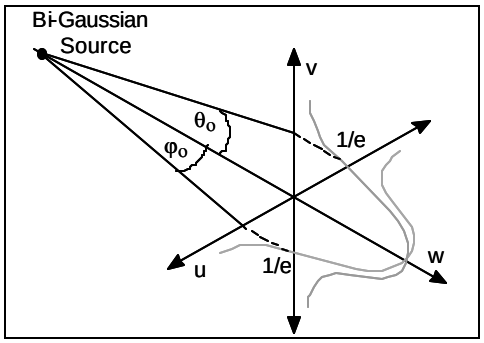

Figure 6: Spatial intensity profile of a beamlet from a bi-Gaussian source

Diodes for pumping HAPSSL are usually manufactured in linear arrays known as "bars." One bar may contain 10 or more individual diodes sharing the same substrate and producing a total output of 20 to 100 W. Bars are equipped with electrical terminals and mounted on heat exchangers. High divergence in the fast axis (normal to the bar plane) makes it more challenging to harness the output of diode arrays for use in many applications of practical interest. To mitigate this problem, some manufacturers incorporate microlenses in their diode bar assemblies to reduce fast axis divergence to as little as a few degrees.

Because the spacing of individual emitters on a bar is much smaller than the distance to the observation point, linear array of discrete diodes can be approximated as a line source of infinitesimal bi-Gaussian emitters. The far-field intensity profile of a beam generated by a single bar of width $2\,u_o$ is then described as

$$p(u,v,w) = \sum_n p(u_n,v,w) = \int_{-u_o}^{u_o} p(u',v,w)\,du' = \frac{P_o}{4\pi^{1/2}\theta_o u_o w}\left\{\mathrm{erf}\left(\frac{u-u_o}{\varphi_o w}\right) + \mathrm{erf}\left(\frac{u+u_o}{\varphi_o w}\right)\right\}\exp -\left(\frac{v}{\theta_o w}\right)^2 \qquad (2)$$

where P_o is the total emitted power by the bar. Simulations of intensity profiles in Figure 7 show that this approximation works very well in the far field (at a distance many times the diode spacing). This means that a uniform intensity can be obtained from an ensemble of discrete sources only few cm downstream from the emitter plane.

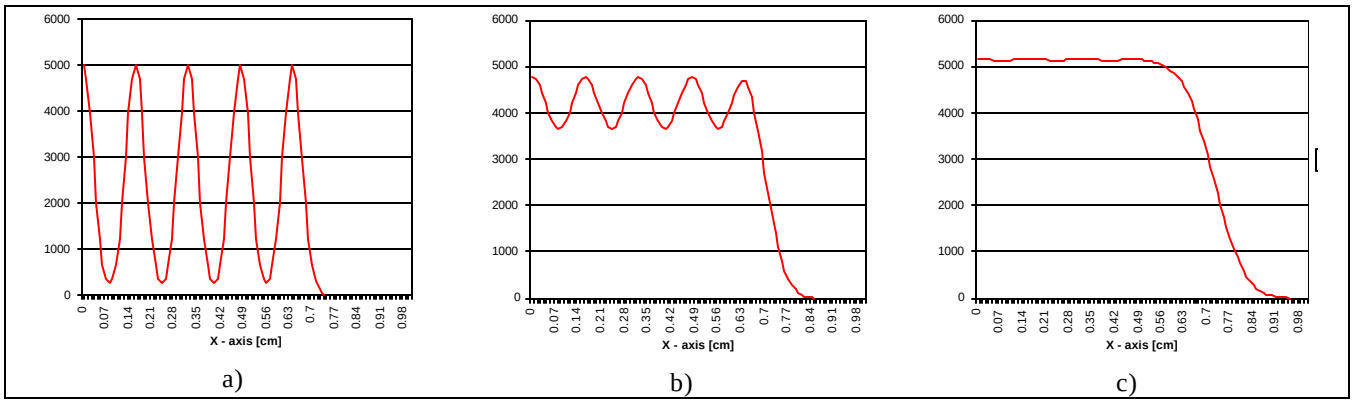

Figure 7: Far-field, mid-plane normalized intensity profile (partial view) generated by an array of 10 discrete diode elements with Gaussian slow-axis divergence 4 deg and fast axis divergence 20 degrees at a distance of a) 1 cm, b) 2 cm, and c) 3 cm away from the emitter plane

Using this analytical foundation, we developed a computational two-dimensional (2-D) model for analysis of pump densities in edge-pumped disk. The disk is assumed to contain an exponentially absorbing laser medium (i.e., obeying Beer's Law). The model is programmed in MATLAB® 6.1 environment and runs on a PC. A PC with a 1-GHz processor can evaluate a typical pump and disk configuration in about 1 minute. Supported diode configurations include the bar width, number of diodes per bar, and bar location with respect to the disk. Outputs of the model include a color-coded plot of absorbed power density, absorbed power density plot in a section through the disk center, power density extreme values, rms value, and standard deviation as a fraction of the rms value. Future updates of this model will accommodate ground-state depletion of the lasing ion [7] and the dynamics of pumping and extraction for quasi-3 level lasants.

To account for diode divergence θ_o in the v-direction (perpendicular to the disk plane), the absorption pathlength is corrected by a factor of $1/\cos(\theta_o/\pi^{1/2})$, Figure 8. The angle $\theta_o/\pi^{1/2}$ is the average "angular component" in the v-direction, which is calculated as

$$\langle|\theta|\rangle = \int |\theta|\, f(\varphi,\theta)\, d\varphi\, d\theta = \frac{1}{\pi\,\theta_o\,\varphi_o} \int_{-\infty}^{\infty} \exp\left[\frac{-\varphi^2}{\varphi_o^{\,2}}\right] d\varphi \; 2\theta_o^{\,2} \int_{0}^{\infty} |\theta| \exp\left[\frac{-\theta^2}{\theta_o^{\,2}}\right] d\theta = \theta_o/\pi^{1/2} \qquad (3)$$

where $f(\varphi,\theta)$ is a distribution function for ray angles emitted by a Gaussian source, namely

$$f(\varphi,\theta) = \frac{1}{\pi\,\theta_o\,\varphi_o} \exp - \left\{\left(\frac{\varphi}{\varphi_o}\right)^2 + \left(\frac{\theta}{\theta_o}\right)^2\right\} \qquad (4)$$

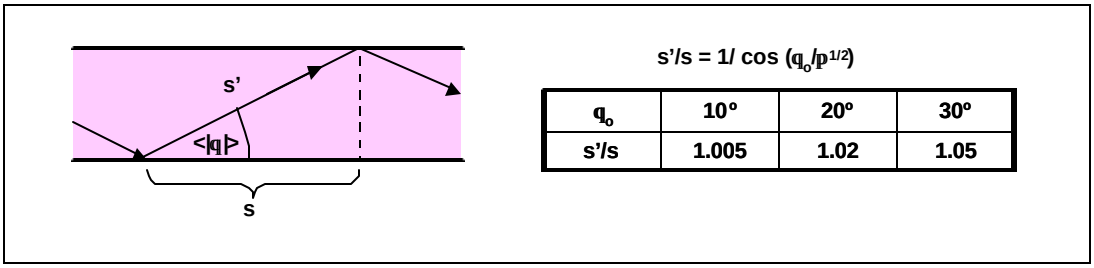

Figure 8: Pathlength correction in the 2-dimensional model

4. PUMP AND GAIN UNIFORMITY STUDIES

Portions of the gain medium disk closer to the diodes are susceptible to being pumped more intensely than portions further away. Nonuniform deposition of pump energy can result in nonuniform gain and loss of beam quality. Achieving high uniformity of gain becomes even more challenging as the incident laser beam may cause saturation-induced change in the spatial gain distribution. For example, the TEM_{oo} laser beam mode has a central peak that would saturate the central portion of the disk and reduce the gain more then in the region near the disk edge. Under these conditions, the weaker portions of the signal would be amplified more than the stronger portions because they saturate the medium to a lesser degree.

In our previous work [5] we have shown that edge-pumped CAMIL exploits the natural divergence of pump diodes to achieve spatially uniform pumping. Beamlets produced by individual laser diode elements overlap inside the gain medium disk and their intensities are summed. Volumetric density of absorbed pump power produced by superposition of multiple beamlets depends on the power output and beamlet divergence of individual diode elements, distance of the diode elements from the disk center, and the density of ground-state ions in the gain medium. It is also affected by the spectral properties of the diodes and the absorption properties of the material, and (to a lesser degree) by the designs of the lensing surface and the concentrator at the disk perimeter.

Figure 9 shows a simple case study performed by the model to illustrate how outputs of multiple diode arrays are used to produce uniform pump field. Figures 10 and 11 show the variation of pump density as a function of diode divergence for several cases of absorption scale length and diode location. Pump density variation is reported as the standard deviation in terms of percentage of rms value.

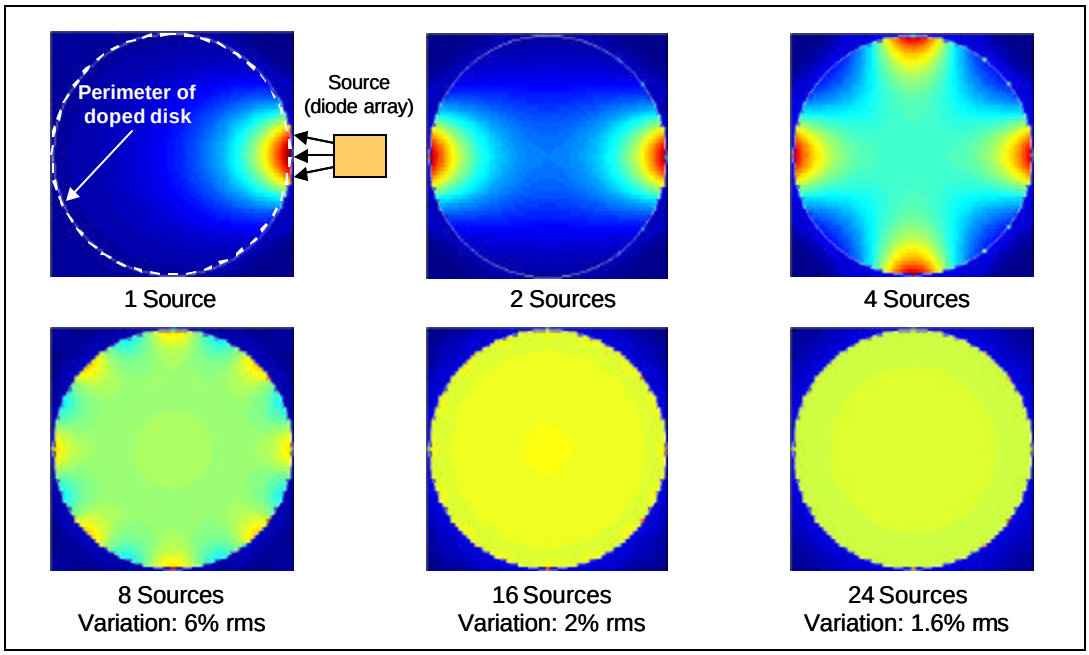

Figure 9: Simulations of absorbed power density showing how outputs of multiple diode array can be used to produce uniform pump field

In all cases shown in Figures 10 and 11, pump density variation initially with increasing diode divergence until it reaches a minimum after which the variation increases with diode divergence. Location of the minimum depends on the disk doping (represented by the absorption scale length x_L) and diode placement. Before reaching a minimum variation, the pump profile exhibits a prominent central peak, whereas after the minimum, there is a shallow central valley. The trend seen in these graphs can be explained as follows. Low divergence diode beamlets overlap mainly in the central portion of the disk, which leads to an intensity maximum there. High

divergence diode beamlets overlap in much of the disk volume but their intensities decrease rapidly both due to spreading and absorption. This causes higher pump intensity near the edge of the disk that is closer to the diodes.

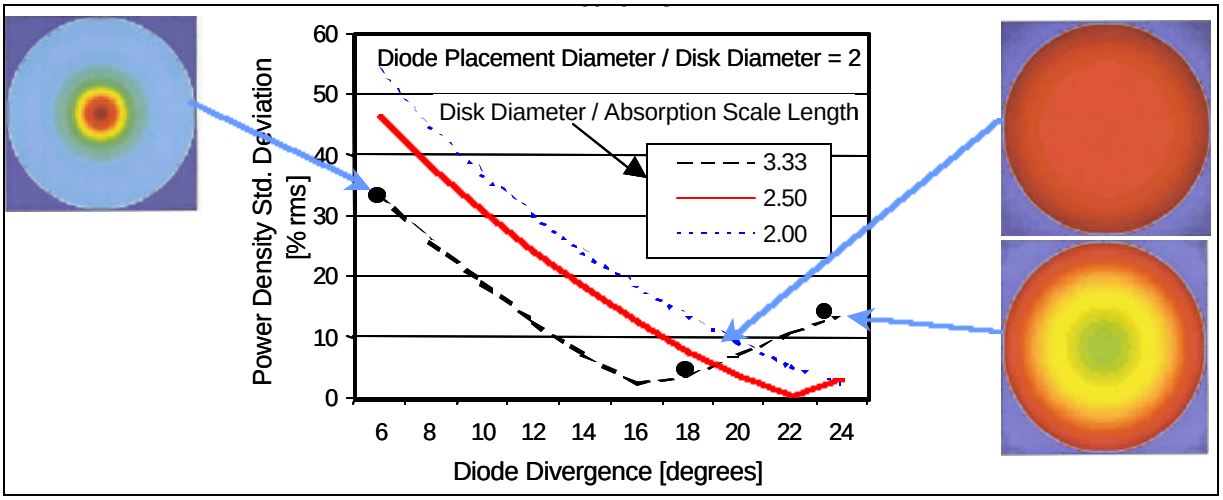

Figure 10: Standard deviation of pump power density in the disk as a percentage of rms absorbed power density versus diode divergence for three cases of absorption scale length and diode placement circle= 2x disk diameter

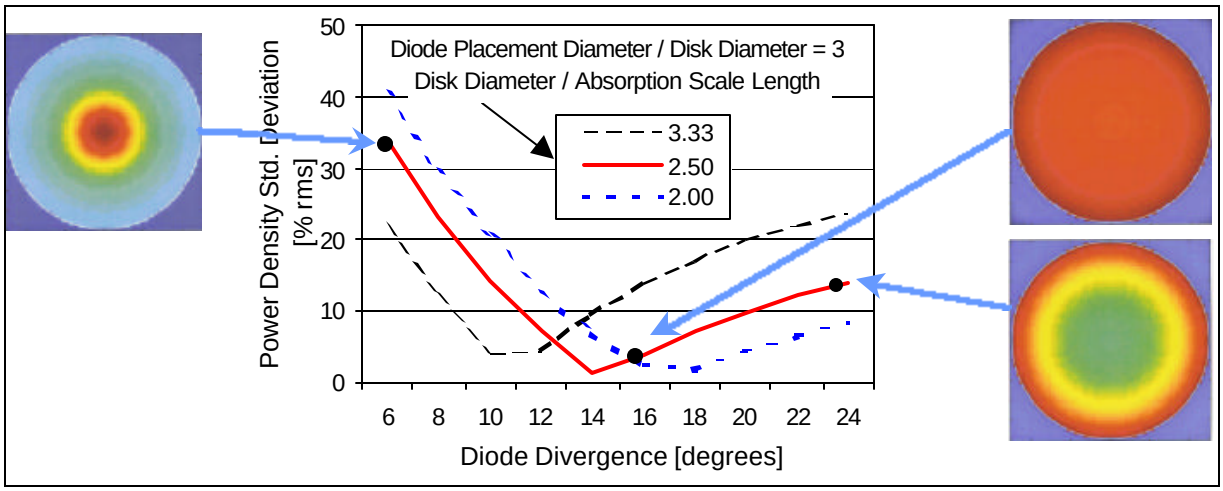

Figure 11: Standard deviation of pump power density in the disk as a percentage of rms absorbed power density versus diode divergence for three cases of absorption scale length and diode placement circle= 3x disk diameter

5. ANALYSIS OF PHASE FRONT DISTORTION

Transverse temperature gradients ($\nabla_{\perp}T$) affect the local optical path and distort the phase front of the incident laser beam. We conducted an analysis using a 2-D MSC/NASTRAN®[1] finite-element model, which revealed two areas of the disk where $\nabla_{\perp}T$ may affect optical path difference (OPD). The first area is near the back face of the disk, where the disk surface facing the microchannel experiences higher heat transfer than the surface contacting the substrate material. As seen in Figure 12, such variations in heat extraction generate small local perturbations to otherwise flat isotherms. We observed that this effect reaches to a depth approximately equal to the width of the microchannels and its strength roughly scales with the ratio of the heat transfer

[1] The MacNeal-Schwendler Corp., Pasadena, CA, USA

coefficient in the microchannel (h_B) and the contact heat transfer coefficient (h_D). Since the contact heat transfer between two optically flat and parallel surfaces is expected to be very good, we have conservatively chosen $h_D = 0.25\ h_B$. Figure 12 shows the OPD for 600-μm channels corresponding to this case. The analysis considered disks made of GGG, YAG, and Q98. For all the materials, the OPD is less than λ/20. Because of if its isothermal properties, Q98 glass shows particularly low sensitivity to microchannel-induced OPD.

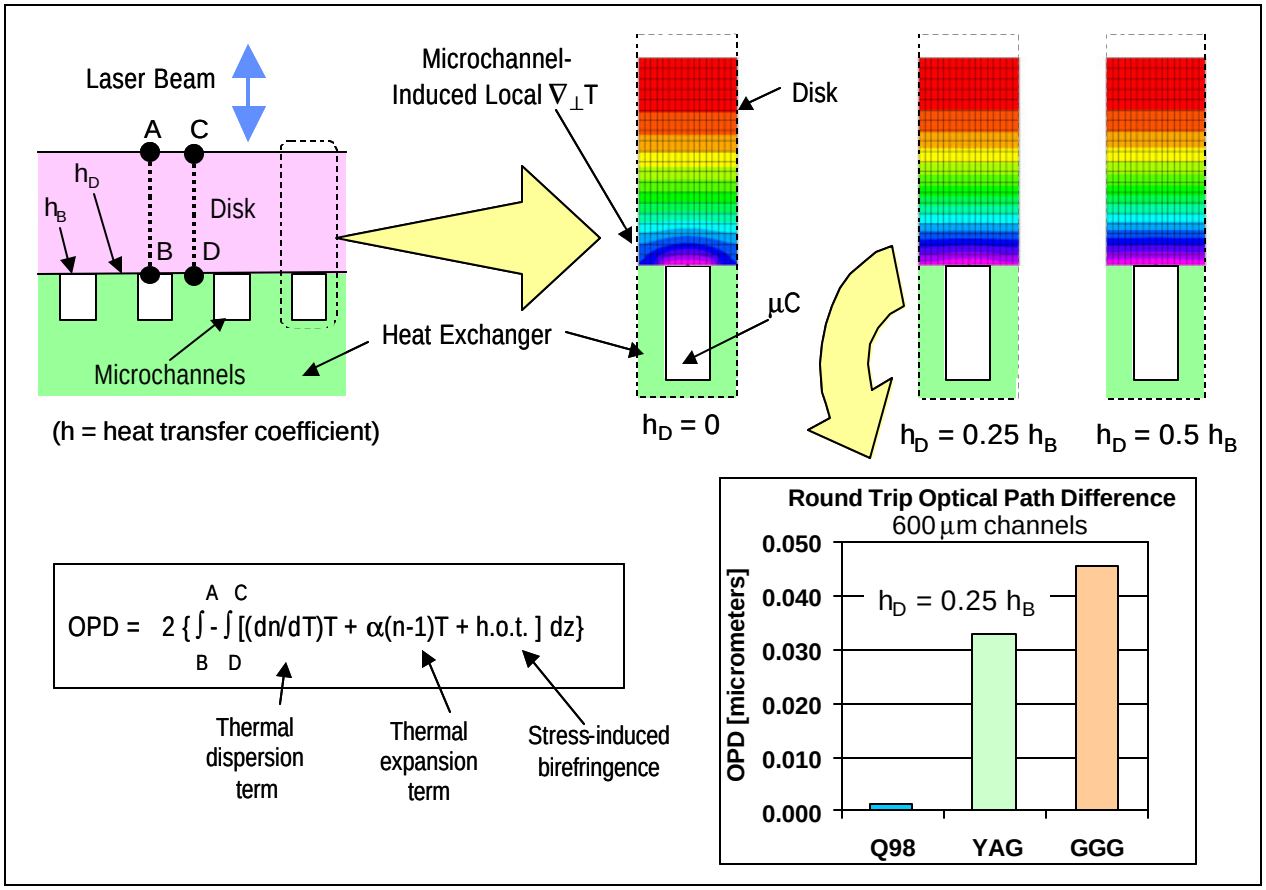

Figure 12: Impact of microchannel-induced $\tilde{N}_\wedge T$ on phase front distortion is very small

The second area potentially causing a wave front distortion is near the edge of the doped disk. The edge experiences a stress concentration caused by an abrupt change in thermal load. As a result, the disk at this location has a tendency to lift off from the substrate. We have previously shown that this tendency can be effectively countered by hydrostatic pressure [4]. In this study, we investigated the relationship between optical flatness of a thermally loaded disk and the applied hydrostatic pressure. The analysis was done using a 3-dimensional (3-D) MSC/NASTRAN® finite element model. Figure 13 shows the results of numerical simulations for a GGG disk indicating that the residual warping effect ("wrinkle") is confined to the disk edge. It can be seen that the central portion of the disk remains flat even as the material has undergone thermal expansion. Therefore, the central portion of the disk provides no contribution to OPD. However, a small region around the disk edge is deformed by both differential thermal expansion and imperfect clamping. The diameter of the central portion of the disk where displacement is under 0.2 μm is about 96% of the doped disk diameter. This means that 92.5% of the doped disk volume is suitable for power extraction with low optical aberration. By increasing the clamping pressure, the wrinkle can be literally "ironed out." Hence, nearly 100% of the pumped volume can be made available for power extraction.

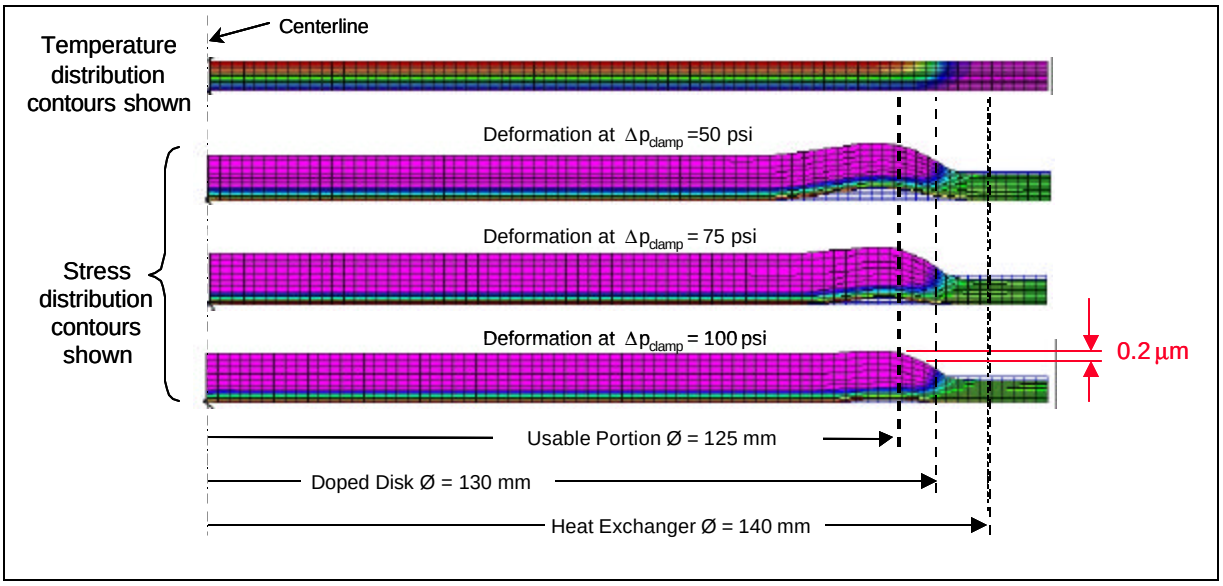

Figure 13: Residual deformations of a Nd:GGG disk near the edge are flattened by increasing pressure (expansion of the disk and deformations are exaggerated in vertical direction)

6. PULSE AMPLIFIER MODEL

One use for CAMIL is in amplification of short pulses. ASE is a major consideration in the design of pulse amplifiers operating in energy storage mode. This is of particular concern in conventional (pass-through) disk amplifiers where ASE photons have a high probability to travel from the source into adjacent amplifier disks. To avoid intolerable loss of gain to ASE, the stored energy is strictly limited and amplifier banks are separated by isolators. In contrast, CAMIL pulse amplifiers such as shown in Figure 14 make it much less likely for ASE photons to travel from disk to disk and depleting the upper state population. This permits operating CAMIL disks at a considerably higher gain then conventional disk amplifiers.

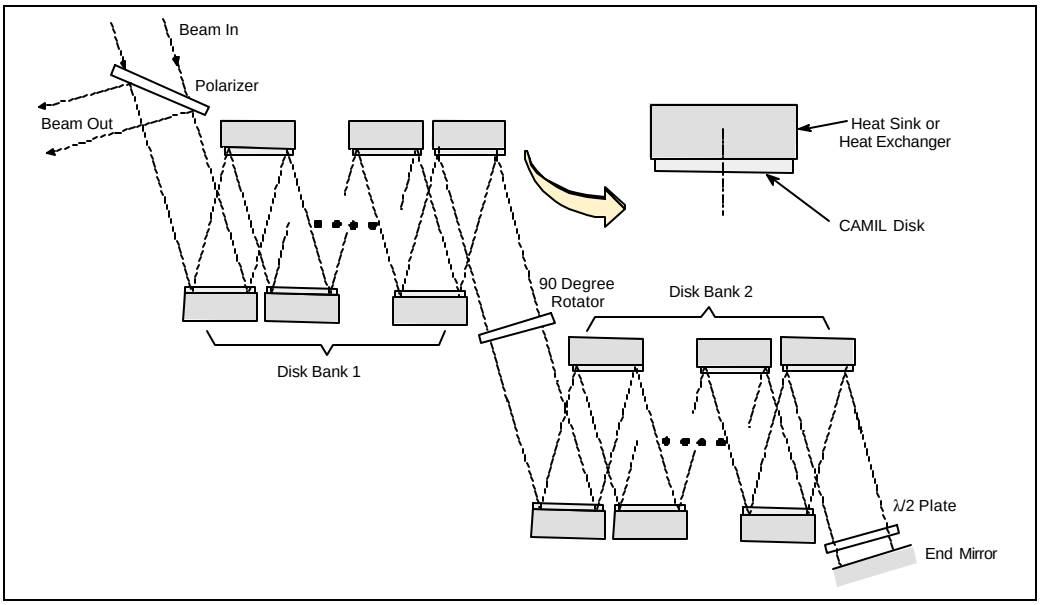

Figure 14: Configuration of short pulse amplifier with two banks of CAMIL disks

Figure 15 shows a prediction of pulse energy growth and extraction efficiency in a CAMIL amplifier using sixteen 5-cm Nd:GGG disks in a double-pass configuration. Each disk experiences four passes which greatly improves extraction efficiency. Figure 16 compares normalized temporal shapes of the injected pulse, pulse at the end mirror, and the output pulse, showing relatively low distortion. Figure 17 shows the output pulse energy and total extraction efficiency for the same amplifier as a function of input pulse energy. An input pulse with flat spatial profile is assumed in all the above cases.

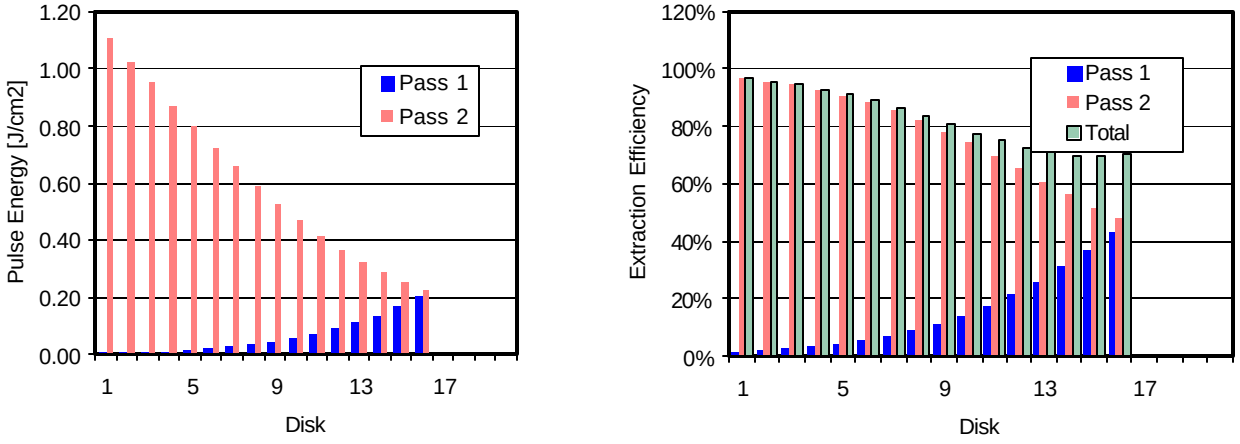

a) *b)*

Figure 15: Predicted a) pulse energy growth and b) extraction efficiency in a CAMIL amplifier using sixteen 5-cm Nd:GGG disks in a double-pass configuration

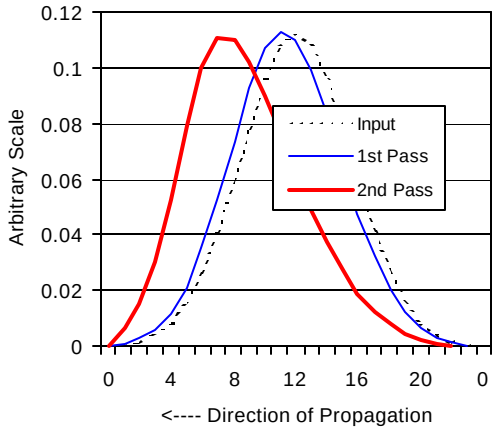

Figure 16: Normalized temporal shapes of the injected pulse, pulse at the end mirror, and the output pulse, showing relatively low distortion.

7. ENGINEERING CONCEPT

To achieve a very compact laser assembly, we developed a configuration with axisymmetric layout of the disks as shown in Figure 18. The number of components is reduced and assembly is simplified by mounting several CAMIL disks onto a common substrate containing internal coolant manifolds. Two such substrates are positioned face-to-face on an optical bench. Figure 19 shows an engineering concept reflecting this approach. The substrates are attached to a cylindrical optical bench that provides sufficient stiffness for maintaining optical alignment under operational dynamic loads. The assembly is further provided with power buses, electric and fluid connections, and placed inside an enclosure protecting the components and maintaining the pressure required for disk attachment.

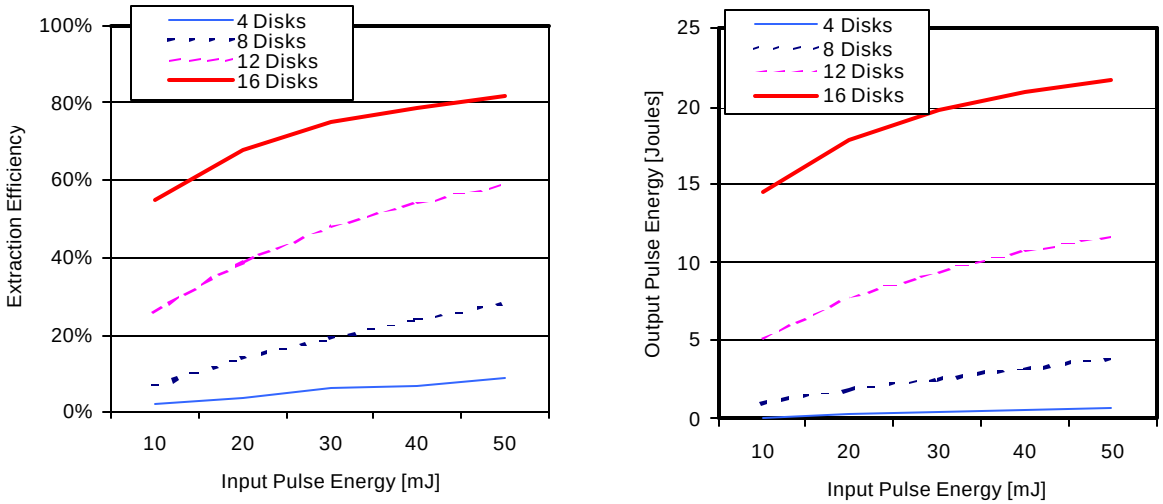

a) b)

Figure 17: Output pulse energy and total extraction efficiency vs. input pulse energy for different numbers of disks

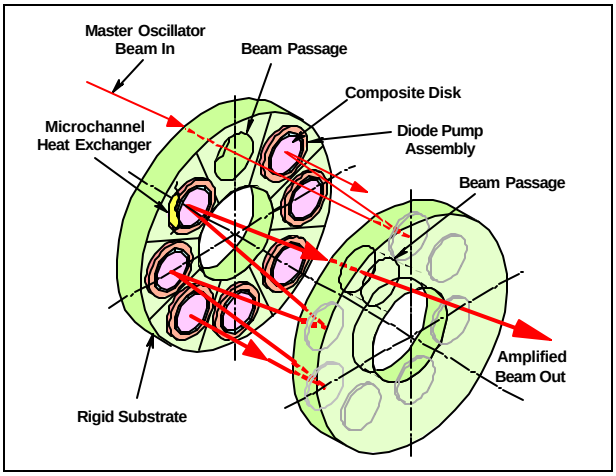

Figure 18: Axisymmetric layout showing multiple disks mounted on a common substrate

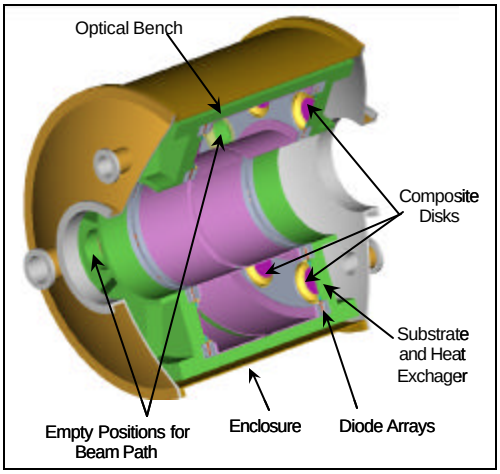

Figure 19: Engineering concept

8. CONCLUSION

We presented an update on the development of a solid-state disk laser in AMA configuration suitable for operation at HAP. The disks are edge-pumped to reduce requirements for doping and pump intensity. A high level of compactness is obtained by mounting multiple disks onto a common substrate. CAMIL disk modules can be used as gain elements in a wide variety of laser oscillator and power amplifier configurations. CAMIL is very suitable for laser material processing requiring HAP and high-brightness such as thick section cutting, deep-penetration welding, cutting and welding of aluminum in the manufacture of aircraft, and drilling of cooling holes in the manufacture of jet engines. Furthermore, 20- to 60-kW beams delivered through optical fibers are also required for thick section cutting in nuclear decontamination and decommissioning. Other emerging applications for ultrahigh-average power SSL include rock drilling for oil and gas exploration, laser power beaming, orbital debris removal, and laser propulsion.

REFERENCES

1. W. Kerchner, "Solid-state laser engineering," chapter 7: "Thermo-optic effects and heat removal," 5th edition, Springer-Verlag, New York, NY, 1999
2. Stewen, K. Contag, M. Larionov, A. Giesen, and H. Hugel, "1-kW CW thin disk laser," *IEEE J. Selected Topics in Quantum Electr*., vol. 6, no. 4, pp. 650-657, July/August 2000
3. L. Zapata, R. Beach and S. Payne, "Composite thin-disk laser scalable to 100 kW average power output and beyond", in the Technical Digest from the Solid State and Diode Laser Technology Review, held in Albuquerque, NM., June 5-8, 2000
4. J. Vetrovec, "Active mirror amplifier for high-average power," SPIE vol. 4270 (2001)
5. J. Vetrovec, "Compact active mirror laser-CAMIL," SPIE vol. 4630 (2002)
6. J. Vetrovec, "Ultrahigh-average power solid-state laser," SPIE vol. 4760 (2002)
7. W. Krupke, "Ground-state depletion lasers," *Optical and Quantum Electronics*, 22 (1990) S1-S22